

Article

Numerical Study of the Morphodynamic Response to a Macro-Scaled Sea-Crossing Project in Hangzhou Bay, China

Wendan Li ^{1,2}, Mingxiao Xie ^{1,2,*}, Heng Wang ^{1,2} and Zhangyi Zhao ^{1,2}

¹ National Engineering Research Center of Port Hydraulic Construction Technology, Tianjin Research Institute for Water Transport Engineering, M.O.T., Tianjin 300456, China

² Key Laboratory of Engineering Sediment of Ministry of Transport, Tianjin Research Institute for Water Transport Engineering, M.O.T., Tianjin 300456, China

* Correspondence: crabsaver@163.com; Tel.: +86-22-59812345 (ext. 6509)

Abstract: Hangzhou Bay is a world-famous strong tidal estuary with an irregular coastline, unique topography, numerous human activities, and complex hydro-sedimentological environment. The Daishan-Yangshan Sea-Crossing Transport Corridor (DSTC) project is located at the mouth of Hangzhou Bay, which is composed of multiple sea-crossing bridges, an underground tube tunnel, and several man-made islands. The large-scale engineering of DSTC fully connects the cities of Shanghai, Yangshan, Daishan, Zhoushan, and Ningbo. This article discusses the morphodynamic responses due to the construction of the DSTC based on a state-of-art numerical model system from the perspective of its impacts on the hydro-sedimentological environment of Hangzhou Bay, as well as on adjacent projects. This study proved that the variation range of tide level in Hangzhou Bay is mostly within 2 cm after the implementation of the DSTC, while that of the man-made island and piers is only within 6 cm. The tidal prism decrease percentage of Hangzhou Bay is less than 0.5%. It does not significantly change the current field and underwater topography in Hangzhou Bay, except near the man-made islands and the bridge. The effect of the DSTC on surrounding ports and channels is small and limited. That is, the proposed DSTC engineering is feasible from the perspective of morphodynamic responses. The conclusions provide a useful reference for similar large-scale estuary construction projects.

Keywords: Hangzhou Bay; numerical model; tidal current; suspended sediment concentration; morphology evolution



Citation: Li, W.; Xie, M.; Wang, H.; Zhao, Z. Numerical Study of the Morphodynamic Response to a Macro-Scaled Sea-Crossing Project in Hangzhou Bay, China. *Water* **2023**, *15*, 1284. <https://doi.org/10.3390/w15071284>

Academic Editors: Tai-Wen Hsu, I-Fan Tseng, Wen-Son Chiang, Wen-Hong Liu, Chung-Ling Chen and Zhi-Cheng Huang

Received: 28 February 2023
Revised: 20 March 2023
Accepted: 22 March 2023
Published: 24 March 2023



Copyright: © 2023 by the authors. Licensee MDPI, Basel, Switzerland. This article is an open access article distributed under the terms and conditions of the Creative Commons Attribution (CC BY) license (<https://creativecommons.org/licenses/by/4.0/>).

1. Introduction

A sea-crossing bridge is a super-large human engineering project across a bay or strait. It may lead to potential hydrodynamic and sediment environmental problems such as tidal level rise [1–3], navigable-flow velocity increases [1,4], excessive siltation in excavated waters [5–8], and significant changes in seabed topography [9–11]. Therefore, scientific research is needed before the implementation of such a super-large project. Its impact should be evaluated and predicted to check its acceptability and optimize the project design to minimize the variation in the tidal currents, sediment transport, as well as the morphology evolution.

Hangzhou Bay is located to the north of Zhejiang Province, south of Shanghai, east of Zhoushan archipelago, and west of Qiantang River (Figure 1). It is a famous trumpet-shaped bay with the largest tidal range in China [12,13]. There are Qijiebamei islands, Tanxushan Island and other islands in the bay, and it covers a water area of approximately 5000 km². From north to south, there are Shengsi islands, Qiqu islands, Chuanhu islands, Daxiaoqushan islands, Huoshan islands, Daishan Island, Daxiaochangtu islands, Xiushan Island, Changbai Island, Zhoushan Island, Cezi Island, Jintang Island, and other islands at the mouth of Hangzhou Bay. Deep tidal channels are usually formed between these

islands, including Dajiyang, Huangzeyang, Daiquyang, Huangdayang, Hengshuiyang and Huibieyang, which are the main channels that connect the Hangzhou Bay with the open sea.

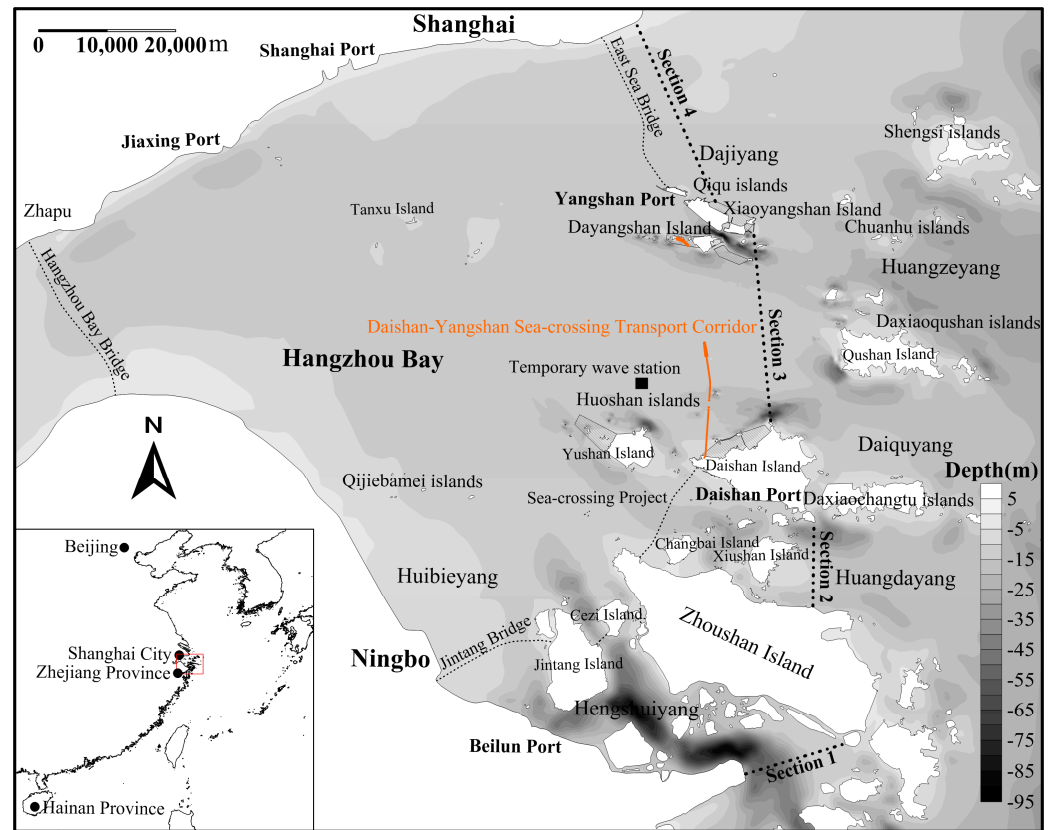


Figure 1. Location of the study area and tidal prism statistical sections (Section 1: Ningbo–Zhoushan Island, Section 2: Zhoushan Island–Daishan Island, Section 3: Daishan Island–Yangshan Island, Section 4: Yangshan Island–Shanghai).

Hangzhou Bay is rich in natural resources such as ports and shipping. In addition to Shanghai Port and Jiaxing Port, there are Daishan Port, Yangshan Port, and Beilun Port. In recent years, with the increasing needs of economic development, a series of high-density artificial engineering construction projects have been carried out in Hangzhou Bay and its adjacent areas. At present, an island connection project from Ningbo to Zhoushan Island and the East Sea Bridge connecting Xiaoyangshan Island and Shanghai have been completed, and the sea-crossing project from Zhoushan Island to Daishan Island has also been started [14]. The DSTC project proposed in this paper achieves the full connection of Ningbo–Zhoushan–Daishan–Yangshan–Shanghai, which is of great significance.

The DSTC project starts from Daishan Island in the south and ends at Dayangshan Island in the north. It intersects with the Daishan North Channel, East Branch of Yushan Bridge Boat Route, Custom Route (West Branch of Yushan Bridge Boat Route), Jinshan Channel (Recommended Route), and Caojingdong Channel in turn (Figure 2a). Apart from the parts of the Daishan North Channel that need to be dredged, the rest are natural channels. The DSTC consists of a 15.0 km long bridge, two man-made islands, and a 14.2 km long underground tunnel between the two man-made islands. The Northern Man-made Island is arranged in a planned reclamation area. The DSTC has about 388 bridge piers with the smallest pier diameter of only 2 m.

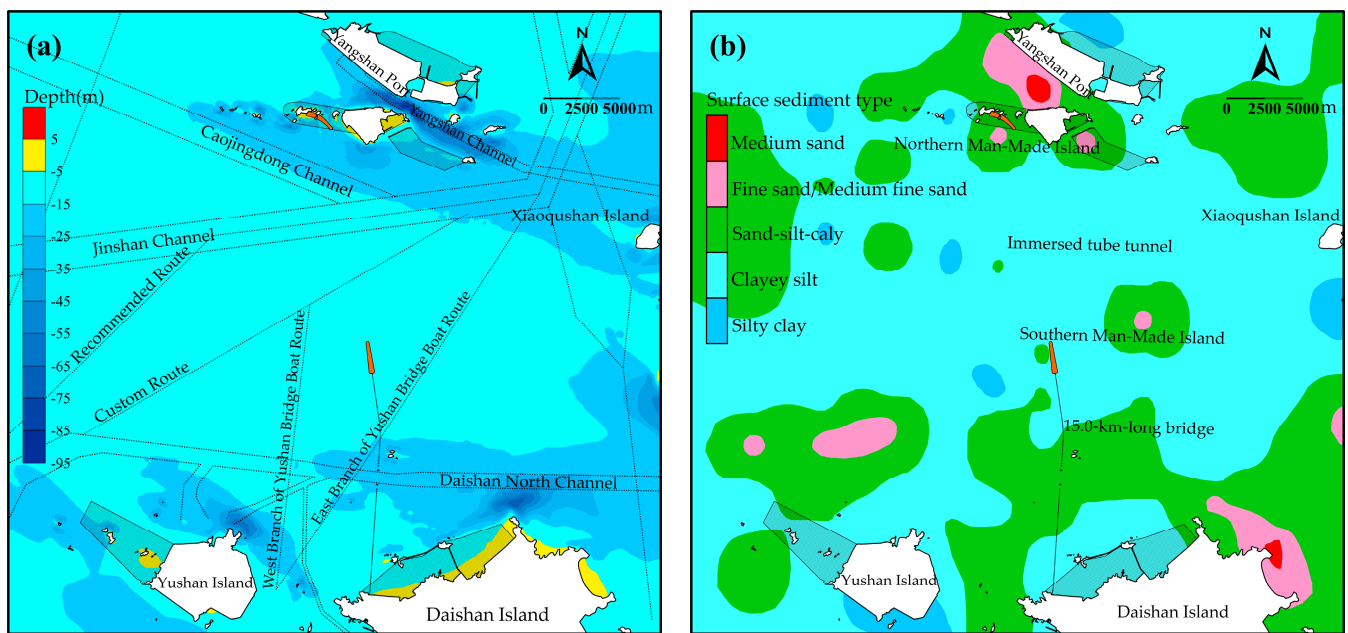


Figure 2. Distribution of present navigation channels and seabed sediment patterns of the studied site. (a) locations of present channels; (b) seabed sediment patterns.

Hangzhou Bay is unique and has more complexity than other bays due to its complex topography and coastline, strong flow dynamics, and high suspended sediment concentration (SSC). Therefore, the bay is of great significance to study the morphodynamic responses of the DSTC for its optimal design. Many existing studies have been carried out on the influence of the construction of a sea-crossing bridge on the hydrodynamic as well as sedimentary environments [15–17]. To date, the numerical model has been an effective tool to simulate the hydrodynamics and sediment movements of the coastal and estuary waters [18–24]. Therefore, in this article we discuss the morphodynamic responses due to the construction of DSTC based on a state-of-the-art numerical model system. Firstly, the hydrodynamics and sediment environment of the engineering sea area were analyzed based on field measurement data. Subsequently, a planar two-dimensional (2DH) model system was established to carry out simulations on the hydro-sedimentological environment under the construction of the DSTC project. In the end, the feasibility of the DSTC was fully evaluated from the perspective of its impacts on hydro-sedimentological environment of Hangzhou Bay, as well as on adjacent projects. In fact, we believe this study provides valuable experience not only as an engineering case study, but also in the construction of similar sea-crossing bridge projects in strong current and high SSC sea areas.

2. Study Area and Methodology

2.1. Study Area

The DSTC project, which connects Daishan Island and Dayangshan Island at the mouth of Hangzhou Bay, belongs to the estuary of Qiantang River. The water depth of deep channels on the south side of Yangshan Island and the north side of Daishan Island is generally between 10 and 30 m, and the water depth between deep channels is basically between 8 and 9 m. The underwater bathymetry near the DSTC presents a distribution trend of shallow water in the middle and deep water on both north and south sides (Figure 2a).

According to the statistical results of the annual measurement data from the wave station on the north side of Yushan Island (Figure 1), the dominant directions are from NNE-SE, with the total occurrence frequency of 61.7%, and the annual average wave height is about 0.7 m.

Due to the limitation of the trumpet-shaped coastline and the increasing bottom friction, the tidal amplitude gradually increases to the upstream along the Hangzhou Bay. In the study site, the average tidal range is between 1.99 and 2.76 m, and the maximum tidal range is between 3.90 and 5.03 m. The tidal current in the Hangzhou Bay belongs to the regular semidiurnal pattern, which is a clockwise reciprocating flow along the coast or deep channels (Figure 3). The tidal current in Hangzhou Bay is strong; therefore, the measured maximum depth-averaged velocities are between 0.71 and 2.51 m/s.

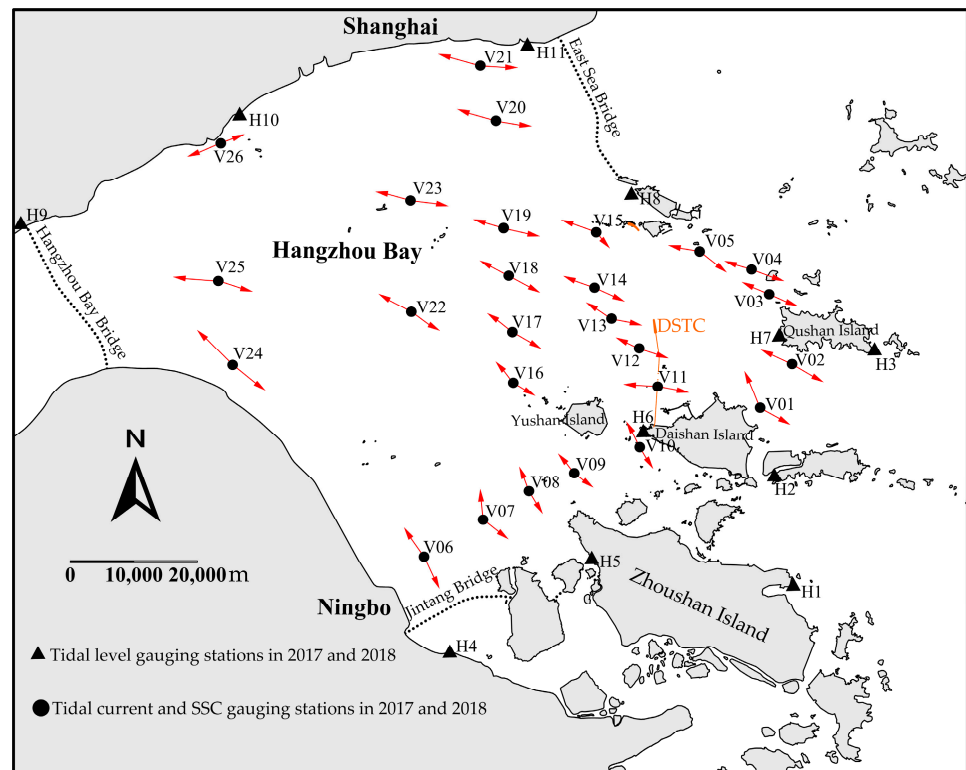


Figure 3. Indication of the main tidal current directions and locations of measurement stations. H1–H11 are the tidal level gauging stations, V1–V26 are the tidal current and suspended sediment concentration gauging stations).

The seabed material of the deep channels on the north side of Daishan Island and the south side of Dayangshan Island are mainly clayey silt and sand-silt-clay. The bed material between the deep channels is mainly clayey silt (Figure 2b). The median bed sediment size d_{50} along the bridge axis of DSTC is 0.01–0.03 mm. The SSC value in the Hangzhou Bay is generally high, which is closely related to the fact that the bed sediments are easily entrained due to strong currents. Along the DSTC area, the mean SSCs range from 0.19 to 2.53 kg/m³.

2.2. Methodology

(1) Governing equations of numerical model

The governing equations of the morphodynamic numerical model system consist of wave propagation, flow movement, suspended sediment transport, and seabed evolution.

$$\frac{\partial N}{\partial t} + \nabla \cdot (\vec{v} N) = \frac{S}{\sigma} \tag{1}$$

$$(c_x, c_y) = \frac{d\vec{x}}{dt} = \vec{c} g + \vec{U} \tag{2}$$

$$c_\sigma = \frac{d\sigma}{dt} = \frac{\partial\sigma}{\partial d} \left[\frac{\partial d}{\partial t} + \vec{U} \cdot \nabla_{\vec{x}} d \right] - c_g \vec{k} \cdot \frac{\partial \vec{U}}{\partial s} \tag{3}$$

$$c_\theta = \frac{d\theta}{dt} = -\frac{1}{k} \left[\frac{\partial\sigma}{\partial d} \frac{\partial d}{\partial m} + k \cdot \frac{\partial \vec{U}}{\partial m} \right] \tag{4}$$

where N is the wave action density; t is the time; $\vec{x} = (x, y)$ is the Cartesian co-ordinate; \vec{v} is the propagation velocity of a wave group; S is the source term for energy balance equation; ∇ is the differential operator; σ is the relative angular frequency; \vec{U} is the current velocity vector; c_g is the magnitude of the group velocity of the wave energy relative to the current; d is the water depth; s is the space co-ordinate in wave direction; θ and m is a co-ordinate perpendicular to s ; \vec{k} is the wave number vector; $\nabla_{\vec{x}}$ is the two-dimensional differential operator in the \vec{x} space.

The tidal current equations are as follows.

$$\frac{\partial h}{\partial t} + \frac{\partial hu}{\partial x} + \frac{\partial hv}{\partial y} = 0 \tag{5}$$

$$\frac{\partial hu}{\partial t} + \frac{\partial hu^2}{\partial x} + \frac{\partial huv}{\partial y} = fvh - gh \frac{\partial \eta}{\partial x} - \frac{h}{\rho_0} \frac{\partial p_a}{\partial x} - \frac{gh^2}{2\rho_0} \frac{\partial \rho}{\partial x} + \frac{\tau_{sx}}{\rho_0} - \frac{\tau_{bx}}{\rho_0} - \frac{1}{\rho_0} \left(\frac{\partial s_{xx}}{\partial x} + \frac{\partial s_{xy}}{\partial y} \right) + \frac{\partial}{\partial x} (hT_{xx}) + \frac{\partial}{\partial y} (hT_{xy}) \tag{6}$$

$$\frac{\partial hv}{\partial t} + \frac{\partial huv}{\partial x} + \frac{\partial hv^2}{\partial y} = -fuh - gh \frac{\partial \eta}{\partial y} - \frac{h}{\rho_0} \frac{\partial p_a}{\partial y} - \frac{gh^2}{2\rho_0} \frac{\partial \rho}{\partial y} + \frac{\tau_{sy}}{\rho_0} - \frac{\tau_{by}}{\rho_0} - \frac{1}{\rho_0} \left(\frac{\partial s_{yx}}{\partial x} + \frac{\partial s_{yy}}{\partial y} \right) + \frac{\partial}{\partial x} (hT_{xy}) + \frac{\partial}{\partial y} (hT_{yy}) \tag{7}$$

where x and y are Cartesian coordinates; η is surface elevation; h is total water depth; u and v are velocity components in the x and y directions, respectively; f is the Coriolis force parameter; g is the gravitational acceleration; ρ_0 is the water density; p_a is the atmospheric pressure; (τ_{sx}, τ_{sy}) and (τ_{bx}, τ_{by}) are the x and y components of the surface wind and bottom shear stresses. $S_{xx}, S_{xy}, S_{yx},$ and S_{yy} are components of wave radiation stresses; T_{xx}, T_{xy} and T_{yy} are components of the lateral stresses which include viscous friction, turbulent friction, and differential advection. In the Cartesian coordinate system (x, y) , the depth-integrated non-equilibrium suspended load equation is listed in Equation (8):

$$\frac{\partial c}{\partial t} + u \frac{\partial c}{\partial x} + v \frac{\partial c}{\partial y} = \frac{1}{h} \frac{\partial}{\partial x} (hD_x \frac{\partial c}{\partial x}) + \frac{1}{h} \frac{\partial}{\partial y} (hD_y \frac{\partial c}{\partial y}) - F_s \tag{8}$$

where c is depth-averaged concentration; D_x and D_y are dispersion coefficients; F_s is the seabed erosion and deposition function. According to Figure 2b, Hangzhou Bay is a typical muddy coast. Sediment movement mainly exists in the form of suspended sediment with little bed load [1,7]. The seabed deformation equation that relates to suspended load is shown in Equation (9):

$$\gamma_0 \frac{\partial \eta_s}{\partial t} - F_s = 0 \tag{9}$$

where γ_0 is sediment dry density; η_s is seabed erosion and deposition thickness.

(2) Model Domain and Mesh Resolution

Because of the extremely complex coastline, it is necessary to establish a large-scale model. The model range is about 280 km × 350 km. There are about 1000 islands in the model domain, and it also considers the upstream discharge of two rivers, which are the Yangtze River and Qiantang River.

The irregular triangular mesh system is adopted to divide the model domain including 137,610 grid nodes and 266,133 elements. The maximum spatial resolution is 10,000 m and

the minimum spatial resolution is 1 m. Each bridge pier is treated as an independent solid boundary (Figure 4). The water depth in the model adopts the sea chart of Hangzhou Bay and the latest local measured data in 2017. The elevation datum system is based on Mean Sea Level.

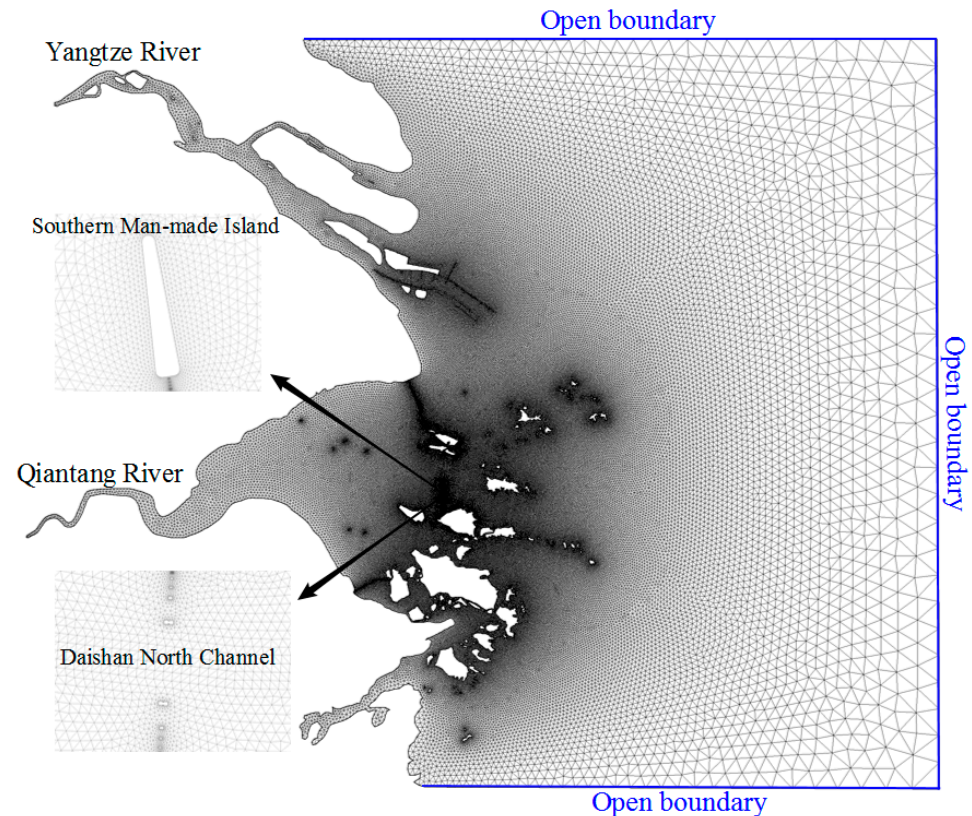


Figure 4. Mesh resolution of the numerical model.

(3) Key parameters

Manning coefficient: The computation domain of this paper is large; thus, the Manning coefficient needs to be calibrated. The final used range of the Manning coefficient is from 60 to 90 $\text{m}^{1/3}/\text{s}$.

Sediment Settling velocity: The typical muds settle in seawater with a form of flocculated mass. The flocculation sediment settling velocity is in the range of 0.04–0.06 cm/s. We take the average value of 0.05 cm/s in this study.

Dry density: The dry density can be determined by the following formula.

$$\gamma_0 = 1750d_{50}^{0.183} \quad (10)$$

where γ_0 is median grain size of the suspended sediment. In this paper, $d_{50} = 0.0078$ mm, so $\gamma_0 = 720$ kg/m^3 .

(4) Open boundary

The open sea tidal level boundary conditions are obtained from the China Tide software [25]. The upstream discharge of Qiantang River is set to the yearly-average value of 1468 m^3/s , and the discharge of Yangtze River is directly set to the measured data provided by the Changjiang Water Resources Commission of the Ministry of Water Resources.

(5) Model calibration

The model was calibrated using four synchronous hydrometric surveys conducted in the Hangzhou Bay in summer (8/2017) and winter (11/2019). There were 11 tidal-level

and 26 tidal-current and SSC stations in each survey (Figure 3). The verification of the calculated results and the measured data of the spring tide in 2017 are shown in Figure 5.

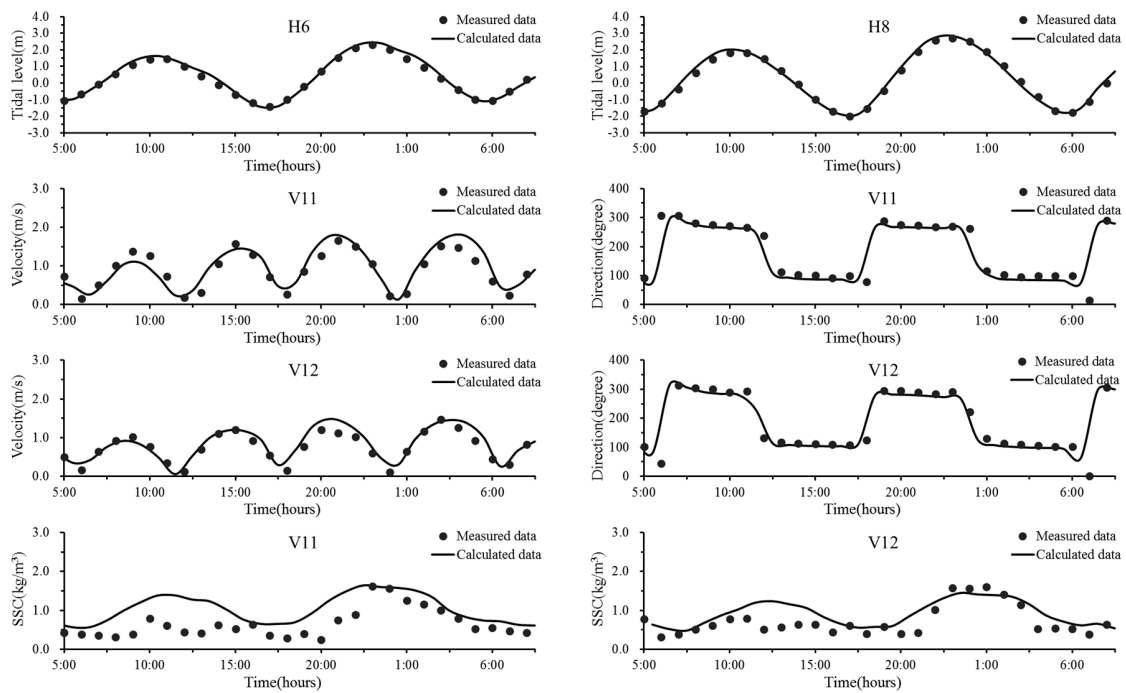


Figure 5. Comparison of calculated data and measured data at representative stations.

The comparison of local depth before and after the implementation of the reclamation project on the north side of Daishan Island (Xiken Hill–Dongken Hill Seawall and Dongken Hill–Daishan Seawall) is suitable for calibrating the seabed deformation (Figure 6).

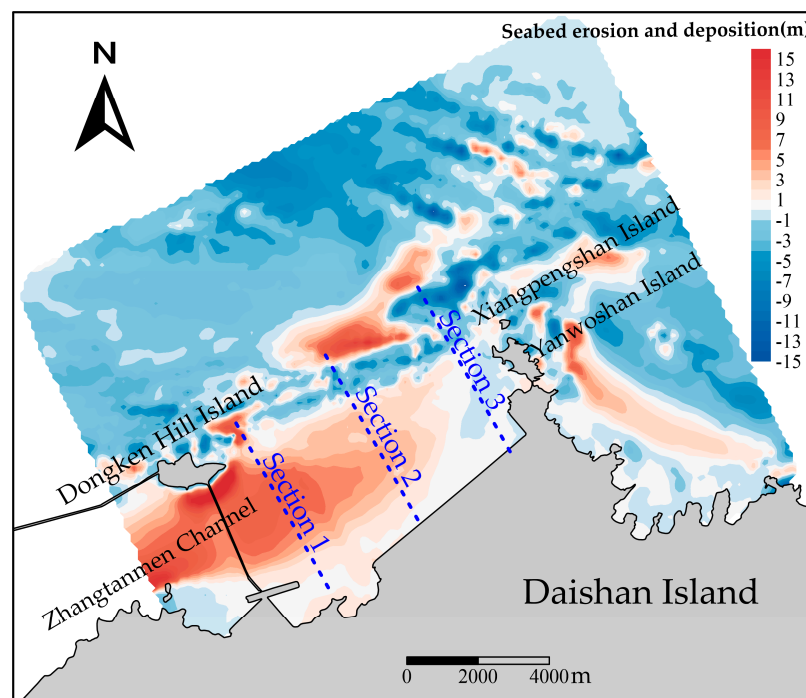


Figure 6. Comparison of local depth before and after the reclamation project of Xiken Hill–Dongken Hill Seawall and Dongken Hill–Daishan Seawall (Sections 1–3 are the selected sections for seabed erosion and deposition verification).

The seabed deformation verification considers the combined effects of waves and tidal currents. The representative wave condition is predicted based on the annual measurement data from the wave station on the north side of Yushan Island. In this paper, the wave direction of WNW-ESE which has great influence on this project is selected as the representative wave. The waves are mainly concentrated in N-NE, ENE-ESE, and WNW-NNW directions, and the total frequency of the three directions is 95 %.

The representative wave height and wave direction are selected according to Equations (11) and (12):

$$\bar{\alpha} = \frac{1}{2} \arcsin \frac{\sum P_i H_i^2 T_i \sin 2\alpha_i}{\sum P_i H_i^2 T_i} \tag{11}$$

$$\bar{H} = \left(\frac{\sum H_i^2 P_i}{\sum P_i} \right) \tag{12}$$

where $\bar{\alpha}$ is the representative wave direction; H_i, T_i, P_i, α_i are wave height, wave period, occurrence frequency and wave direction angle, respectively; \bar{H} is the representative wave height.

Representative and simulated waves characteristics are shown in Table 1. The comparisons of calculated and measured seabed deformation at different sections are shown in Figure 7.

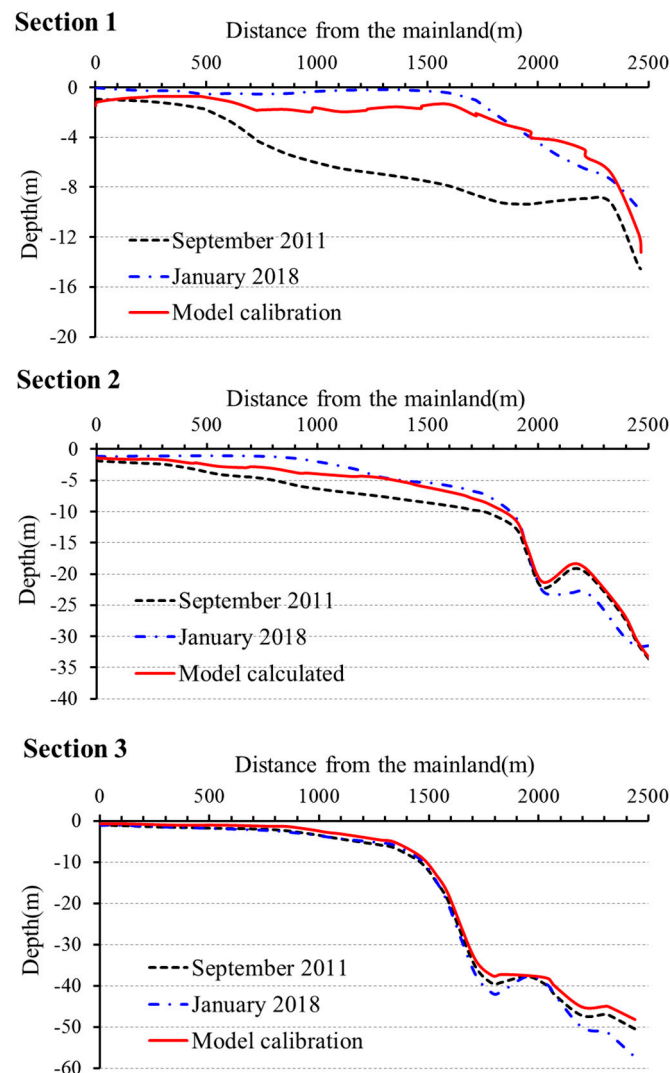


Figure 7. Comparison of calculated and measured seabed deformation at different sections.

Table 1. Representative and simulated waves' parameters.

Parameter	N-NE			ENE-ESE			WNW-NNW		
	Measured	Calculated	Error	Measured	Calculated	Error	Measured	Calculated	Error
Heights (m)	1.01	0.99	−0.02	0.95	0.98	0.03	1.25	1.22	−0.03
Periods (s)	4.4	4.4	0.0	4.3	4.2	−0.1	4.9	5.1	0.2
Directions (°)	20	23	3	89	91	2	318	320	2

3. Results

3.1. Impact on Tidal Level

Numerical simulation results before and after the construction of the DSTC project during spring tide show that the high tide level increases during flood tide and the low tide level decreases during ebb tide on the southeast side of the DSTC, and the high tide level decreases during flood tide and the low tide level increases during ebb tide on the northwest side of the DSTC. These changes in tide levels are more sensitive near the axis of the DSTC. According to the simulation results, the variation range of high and low tide level in Hangzhou Bay is mostly within 2 cm (Figure 8), while that of Southern Man-made Island and piers is only within 6 cm. The numerical simulation results during the spring tide show that the maximum reduction rate of the tidal range near Zhapu (H9 station) is only about 0.37%, which proves that the construction of DSTC has little impact on tidal level.

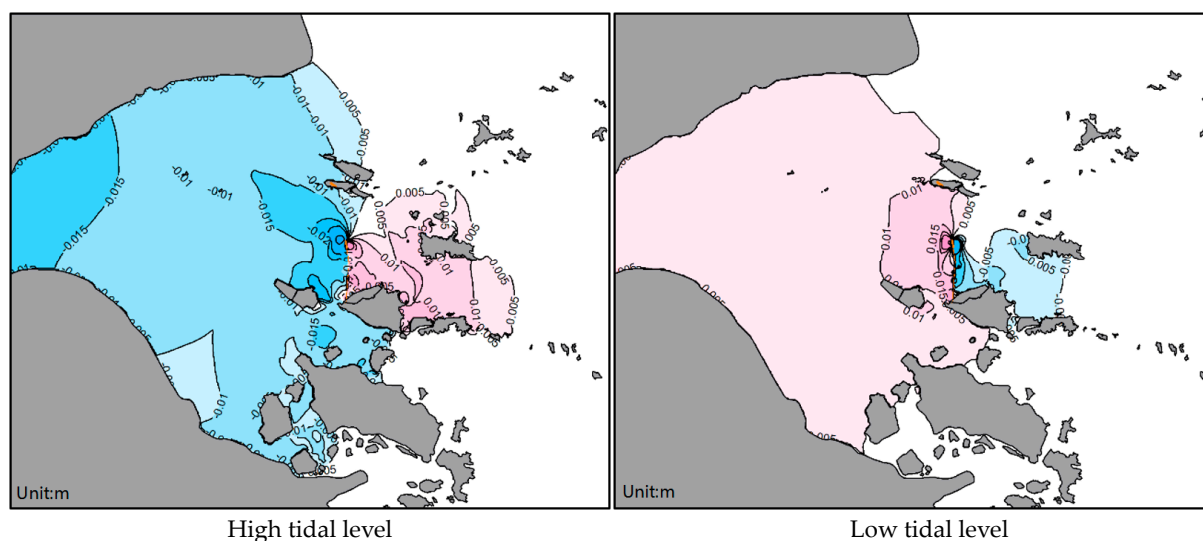


Figure 8. High and low tide level changes (the positive value is the increase in tidal level, and the negative value is the decrease in tidal level).

3.2. Impact on Tidal Prism

The calculated tidal prism changes during spring tide in four sections (S1: Ningbo–Zhoushan Island, S2: Zhoushan Island–Daishan Island, S3: Daishan Island–Yangshan Island, S4: Yangshan Island–Shanghai) before and after the construction of DSTC are listed in Table 2. The tidal prism of Section 1 decreases slightly with the decrease percentage only within 0.10%. The tidal prism of Section 2 and Section 4 increases slightly, and the increase percentage is within 0.11%. The tidal prism of Section 3 tends to decrease, and the decrease percentage is within 1.48%. Generally, the tidal prism decrease percentage in the four sections is less than 0.5%.

Table 2. Variation in tidal prisms (10^8 m^3).

Sections	Flood Tide			Ebb Tide		
	Tidal Prism	Amount of Change	Rate of Change (%)	Tidal Prism	Amount of Change	Rate of Change (%)
Ningbo–Zhoushan Island	94.70	−0.05	−0.05	98.10	−0.10	−0.10
Zhoushan Island–Daishan Island	57.20	0.03	0.05	56.20	0.06	0.11
Daishan Island–Yangshan Island	108.30	−0.97	−0.90	115.50	−1.71	−1.48
Yangshan Island–Shanghai	74.00	0.08	0.11	73.00	0.04	0.05
Ningbo–Shanghai	334.20	−0.91	−0.27	342.80	−1.71	−0.50

3.3. Impact on Current Field and Current Velocity

It can be clearly seen from Figure 9 that the DSTC construction has made no obvious change to the tidal current field in Hangzhou Bay.

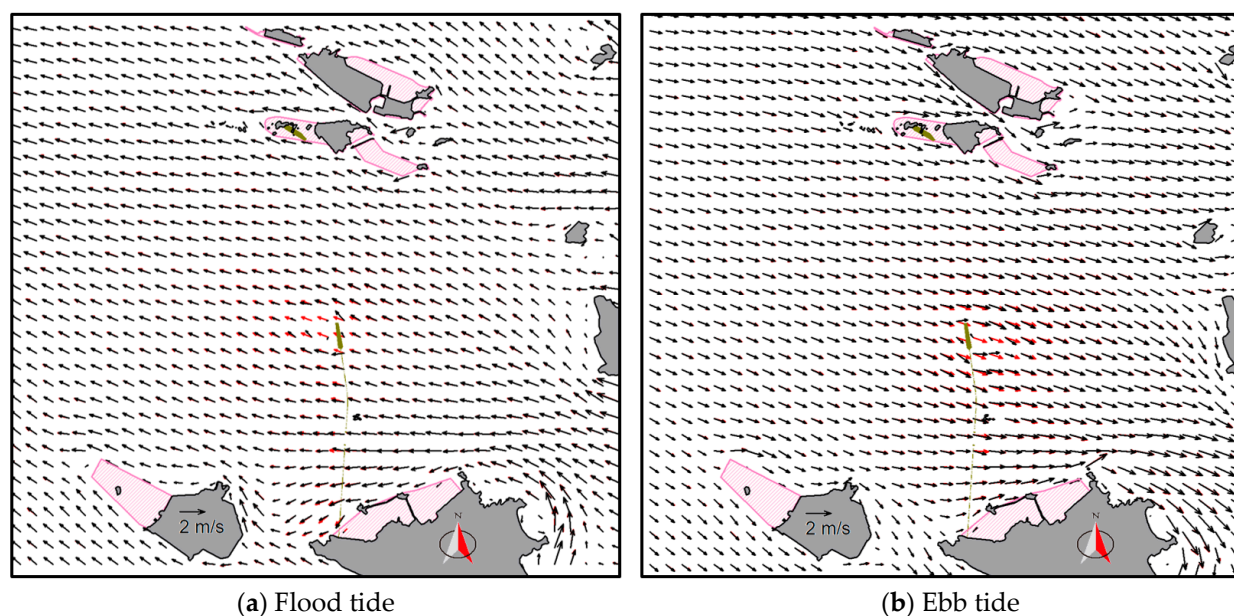


Figure 9. Comparisons of the simulated current fields (red and black arrows are the current fields before and after the DSTC, respectively).

The current fields change obviously near the Southern man-made Island (Figure 10). The current is divided into two branches in the upstream of the Southern man-made Island. Several large-scaled circulation flows form in the downstream with a tongue-like shape, its width is nearly equal to the length of the Southern man-made Island and its length is about 1.2–1.5 times of the length of the Southern man-made Island. The current velocity on the north and south sides of the Southern man-made Island increases sharply, and the maximum value can reach 3.2 m/s.

The current velocity on both sides of the bridge piers decreases due to a water blockage effect (Figure 11). The current velocity in the upstream and downstream of the Southern Man-made Island is significantly reduced, and the decreased value is between 0.01 and 0.75 m/s. The current velocity on the north and south sides of the Southern Man-made Island increases, and the increased value is between 0.01 and 0.67 m/s. The current velocity in the navigable channel of Daishan North Channel increases with a value of 0.14 m/s.

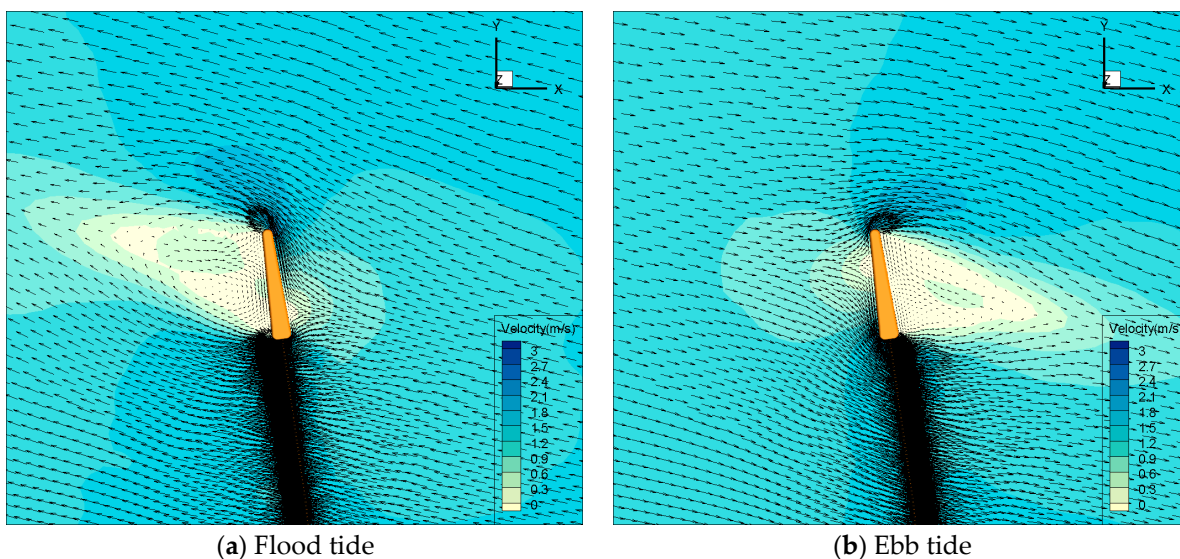


Figure 10. Simulated current fields near the Southern man-made Island.

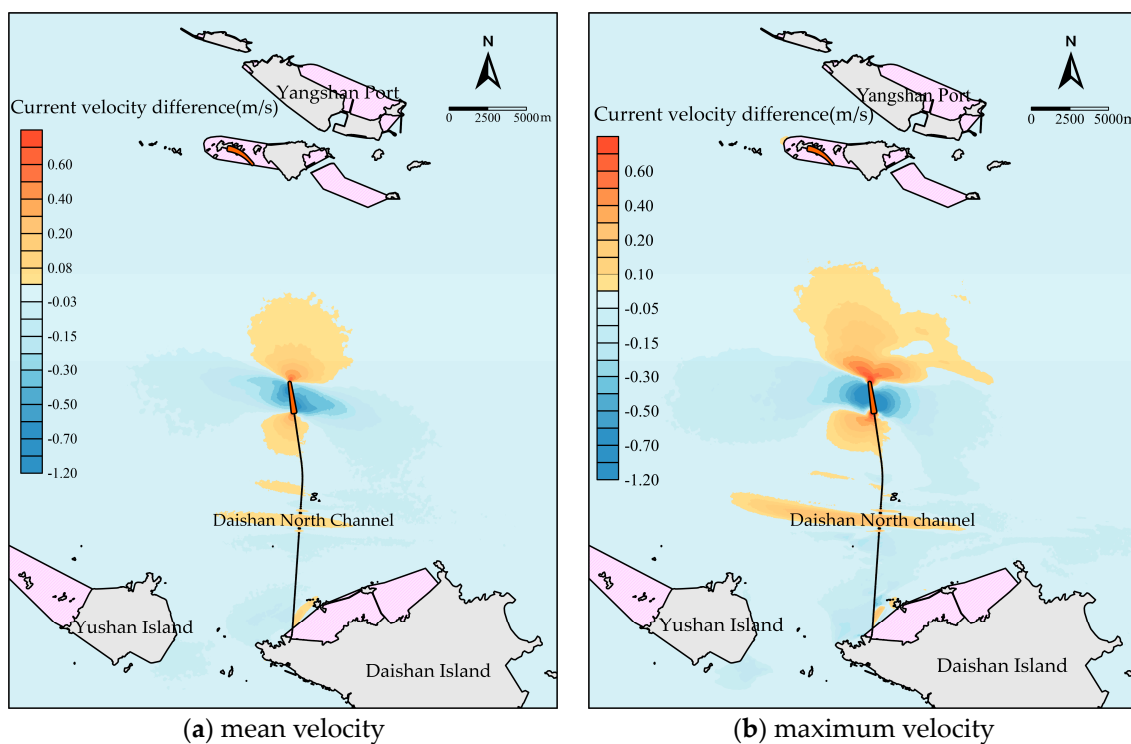


Figure 11. The simulated current velocity difference (The positive value represents the increase in current velocity, and the negative value represents the decrease in current velocity).

3.4. Impact on Morphology Evolution

Driven by the annually averaged wave conditions and upstream discharges, we continuously modeled the hydro-sedimentological processes and predicted the seabed morphology evolution until the morphology reaches the equilibrium state. Figure 12 presents the final stabilized morphology evolution after the construction of DSTC project, and in Figure 13 we also illustrate the evolution time-process of erosion and deposition at two characteristic locations. From the simulation result it can be clearly seen that the rate of seabed erosion and deposition (especially erosion) decreases with time. The seabed erosion and deposition on the west side of Yushan Island and the east side of Daishan Island are basically not affected by the construction of the DSTC. There are obvious seabed deposition

and erosion near the Southern Man-made Island. The maximum erosion thickness and deposition thickness is about 7.6 m and 4.7 m, respectively. The initial development of erosion and deposition is very fast. Over time, the morphology evolution slows down and approximately reaches a stable state of equilibrium in the 8th year.

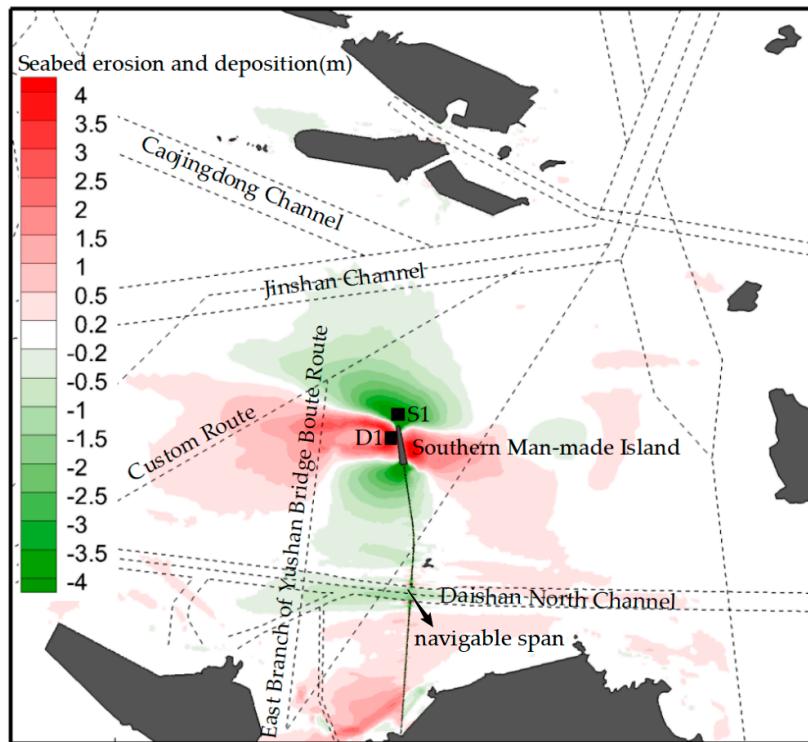


Figure 12. Simulated seabed erosion and deposition thicknesses after the construction of DSTC project. D1 and S1 are locations with maximum deposition and erosion.

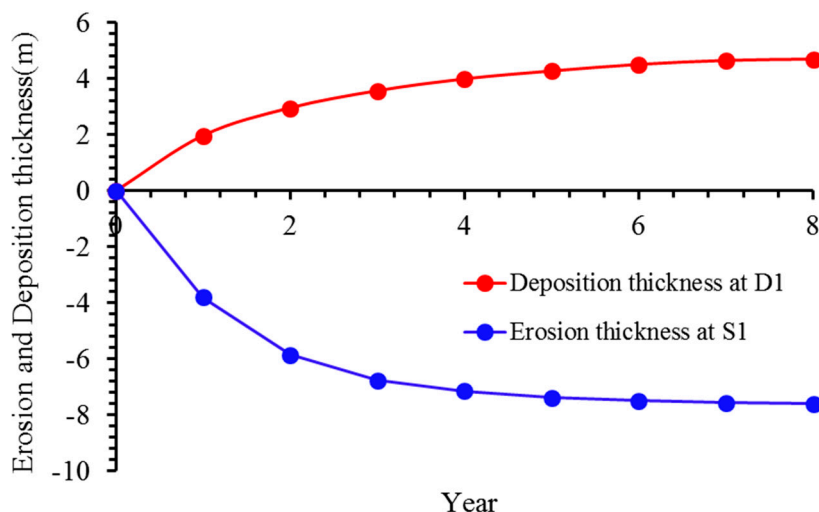


Figure 13. Erosion and deposition process accumulated year by year at sections D1 and S1. The locations of sections D1 and S1 are presented in Figure 12.

The navigable span of the Daishan North Channel generally scours to a maximum thickness of -1.5 m. The seabed deposition occurs at the beaches on both sides of the bridge, and the deposition thickness is between 0.5 and 2.0 m.

3.5. Impact on Harbors and Channels

No influence was found on the Shanghai Port, the Jiaying Port, the Beilun Port, or major channels such as Yangshan Channel, Jinshan Channel, and Caojingdong Channel. Minor influence was found on the Yangshan Port and Daishan Port. The DSTC causes the Daishan North Channel to scour, which is conducive to the maintenance of water depth. There are erosion and deposition on the Custom Route and the East Branch of Yushan Bridge Boat Route. The erosion mainly occurs on the route segment of the north side of the Southern Man-made Island, with the maximum scour thickness of 1.4 m. The deposition mainly occurs on the route segment of the west side of the DSTC, with the deposition thickness within 2.0 m. In summary, the effect of the DSTC on surrounding ports and channels is small and limited.

4. Discussion

There are many islands in the study area (more than 1000 islands), which has an irregular coastline boundary, large tidal range, strong tidal current, and fine seabed material. Therefore, the project area has strong sediment-carrying capacity, high suspended sediment concentration, and complex underwater terrain conditions. Tidal channels with large water depth (local water depth reaches more than 100 m) are often formed between islands due to the narrow channel effect (high tidal current velocity), while muddy tidal flats are developed in tortuous coastline areas where the dynamic condition is weak. In short, there is a close relationship between the water depth and hydrodynamic conditions in the project sea area [10].

The analysis of the simulation results discussed above show that the erosion and deposition mainly occur near the DSTC until the morphology nearly reaches an equilibrium state after approximately 8 years. The east and west sides of the Southern Man-made Island and bridge piers would experience deposition (the maximum deposition thickness is 4.7 m). Two fan-shaped erosion areas form adjacent to the Southern Man-made Island with a maximum erosion thickness of 7.6 m. It is worth noting that deposition mainly occurs in areas with weakened hydrodynamics, while the erosion mainly occurs in the areas with enhanced hydrodynamics. It can be seen that a significant feature of engineering construction on such high suspended sediment concentration coasts is that the hydrodynamic change leads to great changes of morphology while new morphology can also feedback to the hydrodynamics, which is a fully coupled process. This erosion and deposition change developed very fast in the early stage, and the morphological evolution slowed down with the increase of time.

According to the measured bathymetry data (1:25,000), the long-term morphology evolution of the large-scale seabed exhibited a slightly erosive trend during 2011–2017 due to the decrease of upstream sediment supply from the Yangtze River in recent years [26–28]. Therefore, the seabed deformation resulting from the DSTC is impressive compared to natural evolution. Nevertheless, for the entire Hangzhou Bay, the impact of the construction of the DSTC is still limited. The tidal prism decrease percentage is less than 0.5%. In summary, the design of the DSTC is acceptable in terms of its effects on the surrounding hydro-sedimentological environment.

However, it should be emphasized that the problem to be solved in this paper is the impact of DSTC construction on the morphodynamics and hydrodynamics environment in large-scale sea areas. Therefore, the numerical model used in this paper is a two-dimensional large-scale shallow water model, which cannot accurately simulate the fine local three-dimensional flow phenomena such as the horseshoe vortex and local scour depth of the piers [29–32]. Therefore, if we focus on the local scour and protection of bridge piers, it is recommended carrying out additional physical model tests in the future.

5. Conclusions

The DSTC, which is composed of multiple sea-crossing bridges, an underground tube tunnel and several man-made islands, is a challenging large-scale project that is located at

the mouth of Hangzhou Bay, China. Due to the complex shoreline boundaries and unique topographic conditions, strong current velocity, and high suspended sediment concentration, the DSTC may lead to potential morphodynamic responses and raising environmental problems. Scientific research is needed before the implementation of such super-large projects. This article discusses the morphodynamic responses due to the construction of the DSTC based on a state-of-art numerical model system from the perspective of its impacts on hydro-sedimentological environment of Hangzhou Bay, as well as on adjacent projects. In addition, this paper provides a useful resource for similar large-scale estuary construction projects. Based on simulation results and discussions, several conclusions are listed as follows.

(1) The impact of the DSTC on tidal currents is limited to its vicinity except that near the bridge and man-made islands. It has little impact on the tidal level and tidal prism. Once constructed, the variation range of tide level in Hangzhou Bay is within 2 cm, while that of the man-made island and piers is only within 6 cm. The tidal prism decrease percentage of Hangzhou Bay is less than 0.5%;

(2) The seabed scours on the north and south sides of the Southern Man-made Island, whereas it deposits on its east and west upstream and downstream sides. The maximum thicknesses of erosion and deposition around the island is about 7.6 m and 4.7 m, respectively. The initial development of erosion and deposition is very fast. Over time, such change slows down and basically reaches a stable state of equilibrium in 8 years;

(3) The construction of DSTC has no influence on the Shanghai Port, Jiaying Port, Beilun Port, and other major channels such as Yangshan Channel, Jinshan Channel, and Caojingdong Channel. Minor influence was observed in the Yangshan Port, Daishan Port, Custom Route and East Branch of Yushan Bridge Boat Route.

In summary, based on the simulation results, the DSTC design is feasible in terms of the morphodynamic responses, and the morphology evolution reaches equilibrium in 8 years. However, the numerical model applied in this article is 2DH, which is more suitable for estimating morphodynamics on a large scale. If we focus on a more delicate process e.g., the local scour at bridge piers, a physical model or CFD numerical model is more appropriate.

Author Contributions: Writing—original draft, W.L.; methodology, M.X.; writing—review and editing, H.W. and Z.Z.; funding acquisition, M.X. All authors have read and agreed to the published version of the manuscript.

Funding: The work presented in this paper is financially sponsored by the National Natural Science Foundation of China (52171260, 42006153), the Research Innovation Fund of Tianjin Research Institute for Water Transport Engineering (TKS20230501, TKS20220203), and the Young Elite Scientists Sponsorship Program by CAST (2021QNRC001).

Data Availability Statement: Not applicable.

Conflicts of Interest: The authors declare no conflict of interest.

References

1. Li, M.G.; Li, W.D.; Xie, M.X. Morphodynamic Responses to the Hong Kong-Zhuhai-Macao Bridge in the Pearl River Estuary. *J. Coast. Res.* **2021**, *37*, 168–178. [[CrossRef](#)]
2. Gong, Z.; Zhang, C.K.; Wan, L.M.; Zuo, J.C. Tidal Level Response to Sea-Level Rise in the Yangtze Estuary. *Chin. Ocean Eng.* **2012**, *26*, 109–122. [[CrossRef](#)]
3. He, M.; Xu, W.H.; Gao, X.F.; Ren, B. The layout of submerged horizontal plate breakwater (SHPB) with respect to the tidal-level variation. *Coast. Eng. J.* **2018**, *60*, 280–298. [[CrossRef](#)]
4. Luo, Z.J.; Wu, J.Z.; Hu, R.J.; Zhu, L.H. Characteristics of Erosion and Deposition in Dongying Harbor Area. *Mar. Geol. Front.* **2016**, *32*, 40–45.
5. Lu, Y.J.; Ji, R.Y.; Zuo, L.Q. Morphodynamic responses to the deep water harbor development in the Caofeidian sea area, China's Bohai Bay. *Coast. Eng.* **2009**, *56*, 831–843. [[CrossRef](#)]
6. Schmeckle, M.W. Numerical simulation of turbulence and sediment transport of medium sand. *J. Geophys. Res. Earth Surf.* **2014**, *119*, 1240–1262. [[CrossRef](#)]

7. Zuo, S.H.; Li, B. Study on hydrodynamic and sedimentation problems in development of harbors located at offshore area with many islands and tidal channels. *J. Hydrodyn.* **2010**, *22*, 587–592. [[CrossRef](#)]
8. Hu, C.H.; Ji, Z.W.; Guo, Q.C. Flow movement and sediment transport in compound channels. *J. Hydraul. Res.* **2010**, *48*, 23–32. [[CrossRef](#)]
9. Lu, Y.J.; Zuo, L.Q.; Ji, R.Y.; Liu, H.X. Deposition and erosion in the fluctuating backwater reach of the Three Gorges after upstream reservoir adjustment. *Int. J. Sediment Res.* **2010**, *25*, 64–80. [[CrossRef](#)]
10. Hou, Q.Z.; Wang, Z.L.; Lu, Y.J.; Mo, S.P. The morphodynamic responses to deposition-promoting projects in island and reef coasts of the Zhoushan Archipelago, China. *Int. J. Sediment Res.* **2017**, *32*, 351–363. [[CrossRef](#)]
11. Han, Z.Y.; Xie, H.L.; Li, H.Y.; Xie, M.X. Morphological Evolution of the Lingding Channel in the Pearl River Estuary over the Last Decades. *J. Coast Res.* **2020**, *37*, 104–112. [[CrossRef](#)]
12. Pan, C.H.; Zheng, J.; Zheng, G.; He, C.Q.; Tang, Z.W. Spatial and Temporal variations of tide characteristics in Hangzhou Bay and cause analysis. *Ocean Eng.* **2019**, *37*, 1–11.
13. Pan, C.H.; Zheng, J.; Wu, X.G.; Chen, G. Spatiotemporal variation of annual maximum high tide levels and reason analysis for their uplifting in Hangzhou Bay. *J. Hohai Univ. (Nat. Sci.)* **2021**, *49*, 394–418.
14. Liu, Y.; Yu, B.N.; Zhou, R. Study of Strategic Planning for the Zhoushan-Shanghai Sea-crossing Transport Corridor. *High Way* **2020**, *10*, 216–223.
15. Han, H.Q.; Xiong, S.L.; Zhu, J.Z.; Yu, Y.Y.; Zeng, J.; Chen, W. The impact on the flow of Qiantang Estuary by the Hangzhou Bay Major Bridge. *Donghai Mar. Sci.* **2002**, *20*, 57–63.
16. Huang, Y.M.; Wang, P.G.; Zhao, M.; Zhang, C.; Du, X.L. Dynamic response of sea-crossing bridge under combined seismic and wave-current action. *Structures* **2022**, *40*, 317–327.
17. Ti, Z.; Wei, K.; Qin, S.; Mei, D. Numerical simulation of wave conditions in nearshore island area for sea-crossing bridge using spectral wave model. *Adv. Struct. Eng.* **2018**, *21*, 756–768. [[CrossRef](#)]
18. Zeng, X.G.; He, R.Y.; Xue, Z.; Wang, H.J.; Wang, Y.; Yao, Z.; Guan, W.B.; Warrillow, J. River-derived sediment suspension and transport in the Bohai, Yellow, and East China Seas: A preliminary modeling study. *Cont. Shelf Res.* **2015**, *111*, 112–125.
19. Pan, C.H.; Lin, B.Y.; Mao, X.Z. Cause Study: Numerical Modeling of the Tidal Bore on the Qiantang River, China. *J. Hydraul. Eng.* **2007**, *133*, 130–138. [[CrossRef](#)]
20. Wu, W.; Rodi, W.; Wenka, T. 3D numerical modeling of flow and sediment transport in open channels. *J. Hydraul. Eng.* **2000**, *126*, 4–15. [[CrossRef](#)]
21. Fang, G.; Yang, J.; Thao, Y. A two-dimensional numerical model for tidal motion in the Taiwan Strait. *Mar. Geophys. Res.* **1984**, *7*, 267–276. [[CrossRef](#)]
22. Frey, A.E.; Connell, K.J.; Hanson, H.; Larson, M.; Thomas, R.C.; Munger, S.; Zundel, A. *GenCade Version 1 Model Theory and User's Guide*; Engineer Research and Development Center Vicksburg Ms Coastal Inlets Research Program; Defense Technical Information Center: Fort Belvoir, VA, USA, 2012.
23. Tomasicchio, G.R.; Francone, A.; Simmonds, D.J.; D'Alessandro, F.; Frega, F. Prediction of shoreline evolution. Reliability of a general model for the mixed beach case. *J. Mar. Sci. Eng.* **2020**, *8*, 361. [[CrossRef](#)]
24. Villaret, C.; Hervouet, J.M.; Kopmann, R.; Merkel, U.; Davies, A.G. Morphodynamic modeling using the Telemac finite-element system. *Comput. Geosci.* **2013**, *53*, 105–113. [[CrossRef](#)]
25. Li, M.G.; Zheng, J.Y. Introduction to Chinatide software for tide prediction in China seas. *J. Waterw. Harb.* **2007**, *28*, 65–68.
26. Yang, H.F.; Yang, S.L.; Xu, K.H.; Milliman, J.D.; Wang, H.; Yang, F.; Chen, Z.; Zhang, C.Y. Human impacts on sediment in the Yangtze River: A review and new perspectives. *Glob. Planet. Change* **2018**, *162*, 8–17. [[CrossRef](#)]
27. Yang, S.L.; Xu, K.H.; Milliman, J.D.; Yang, H.F.; Wu, C.S. Decline of Yangtze River water and sediment discharge: Impact from natural and anthropogenic changes. *Sci. Rep.* **2015**, *5*, 12581. [[CrossRef](#)]
28. Dai, Z.J.; Liu, J.; Xie, H.L.; Shi, W.Y. Sedimentation in the outer Hangzhou Bay, China: The influence of Changjiang sediment load. *J. Coast. Res.* **2014**, *30*, 1218–1225. [[CrossRef](#)]
29. Han, H.Q.; Xiong, S.L.; Sun, Z.L. Local scour equation at bridge piers under tidal current action. *J. Sediment Res.* **2016**, *1*, 9–13.
30. Xiong, W.; Zhang, X.F.; Tang, P.B.; Wang, B.; Ye, J.S. Scour condition analysis on pylons of Hangzhou Bay by tracing dynamic behaviors of superstructures. *J. Southeast Univ. (Nat. Sci. Ed.)* **2018**, *48*, 871–877.
31. Sheppard, D.M.; Melville, B.; Demir, H. Evaluation of existing equations for local scour at bridge piers. *J. Hydraul. Eng.* **2014**, *140*, 14–23. [[CrossRef](#)]
32. Qi, M.; Li, J.; Chen, Q. Comparison of existing equations for local scour at bridge piers: Parameter influence and validation. *Nat. Hazards* **2016**, *82*, 2089–2105. [[CrossRef](#)]

Disclaimer/Publisher's Note: The statements, opinions and data contained in all publications are solely those of the individual author(s) and contributor(s) and not of MDPI and/or the editor(s). MDPI and/or the editor(s) disclaim responsibility for any injury to people or property resulting from any ideas, methods, instructions or products referred to in the content.